RSC Advances

This is an *Accepted Manuscript*, which has been through the Royal Society of Chemistry peer review process and has been accepted for publication.

Accepted Manuscripts are published online shortly after acceptance, before technical editing, formatting and proof reading. Using this free service, authors can make their results available to the community, in citable form, before we publish the edited article. This *Accepted Manuscript* will be replaced by the edited, formatted and paginated article as soon as this is available.

You can find more information about *Accepted Manuscripts* in the Information for Authors.

Please note that technical editing may introduce minor changes to the text and/or graphics, which may alter content. The journal's standard Terms & Conditions and the Ethical guidelines still apply. In no event shall the Royal Society of Chemistry be held responsible for any errors or omissions in this *Accepted Manuscript* or any consequences arising from the use of any information it contains.

ROYAL SOCIETY OF CHEMISTRY

www.rsc.org/advances

Theoretical investigation of H_2S removal on the γ-Al_2O_3 surfaces of different hydroxyl coverage

Rui-Peng Ren, Xiao-Wei Liu, Zhi-Jun Zuo* and Yong-Kang Lv*

Key Laboratory of Coal Science and Technology of Ministry of Education and Shanxi Province, Taiyuan University of Technology, Taiyuan 030024, Shanxi China

***Corresponding author. Fax: +86 351 6010386.**

Abstract: The sulfurized processes of H_2S on dehydrated (100) and (110) as well as partially hydrated (110) surfaces of γ-Al_2O_3 have been investigated by using periodic density functional theory method. The adsorption configurations of possible intermediates and the potential energy profiles of reaction are depicted. Our results show that H_2S is preferred to adsorb on the Al site along with S bond, and the adsorption energies are –32.52 and –114.38 kJ/mol on the dehydrated (100) and (110) surfaces, respectively. As the changes of reaction temperature of the desulfurization, the (110) surface presents the different levels of hydroxyl coverage which affects the adsorption structures of species and reaction energies of dissociation processes. It is found that the bonding strengths of H_2S on the partially hydrated (110) surfaces are weaker than that of on the dehydrated (110) surface. Comparing with the 3.0 and 8.9 OH nm^{-2} surfaces, the H_2S has the weakest adsorption energy (–39.85 kJ/mol) and the highest activation energy (92.06 kJ/mol) on the 5.9 OH nm^{-2} surface. On the 8.9 OH nm^{-2} surface, the activation energy of the second dissociation step (rate-determining step) for H_2S dissociation merely is 38.32 kJ/mol. On these involved surfaces, the two H–S bonds cleavage processes present the facile activation energies, which are facilitative to carry out the desulfurization.

Key words: Hydrogen sulfide; γ-Al_2O_3; Density functional theory

RSC Advances Accepted Manuscript

1. Introduction

Hydrogen sulfide (H_2S) is the most common sulfur-containing impurity in combustion of fossil fuels and industrial processes, petroleum/natural gas drilling and refining, coal gasification processes, and biogas generated from anaerobic fermentation of wastes.[1-4] It is pre-requisite to reduce the H_2S content from these streams to meet a low level since they are extremely malodorous and toxic, being as the sources of acid rain, causing pipeline corrosion and limiting plant lifetime,[5, 6] as well as poisoning most downstream catalysts.[7]

Solid metal-oxide sorbents as candidate desulfurization sorbents have been reported extensively to use for removing H_2S, such as CaO, Fe_2O_3, CuO, ZnO, γ-Al_2O_3 and CeO_2.[8-14] Among these metal oxides, γ-Alumina (γ-Al_2O_3) has attracted considerable attention due to the highly efficient desulfurization capability.[15, 16] Meanwhile, γ-Al_2O_3 has been widely used in industrial fields, including as a catalyst support or, as a catalyst (for the Claus process),[17] which is inevitable to react with H_2S in this potential sulfidation environment.[18, 19] Hence, it is significant to understand the detailed reaction process between the γ-Al_2O_3 surface and H_2S. More importantly, the research of surface reaction may be helpful to improve the performance of the desulfurizer. Many attempts have been reported to investigate the interaction mechanism of H_2S with γ-Al_2O_3. Experimentally, adsorption of H_2S on γ-Al_2O_3 surface has been studied using many instruments.[15, 20-24] For example, Travert et al. studied the interaction of H_2S on γ-Al_2O_3 surface by using the infrared (IR) spectroscopy,[25] and the result showed that the adsorption of H_2S irreversibly perturbs the high-frequency region of the IR spectroscopy and results in the changes of surface acidity. DeRosset et al. [26] estimated that isosteric heats of adsorption of H_2S ranged from –104.6 to –159.0 kJ/mol, depending on the degree of dehydration of the γ-Al_2O_3. And entropy calculations indicate

RSC Advances Accepted Manuscript

that mobility of the adsorbed H_2S is highly restricted. Reshetenko et al. [16] have carried out the heterogeneous decomposition of H_2S on γ-Al_2O_3, and found that the reaction order and effective activation energy were determined to be 2.0 and 72 kJ/mol, respectively.

Recently, the density functional theory (DFT) method based on quantum chemistry, as a fairly favorable supplementary experimentally, can provide some molecular and atomic level information which include the positions and behaviors of sulfur components on the γ-Al_2O_3 surface. Arrouvel et al. [27] have investigated the interaction between H_2S and the γ-Al_2O_3 surface under the usual hydrodesulfurization (HDS) conditions by using DFT combined with surface thermochemistry. They pointed out that only rather high temperatures and very low water partial pressure stabilize the sulfidation of the (110) surface, leading to the formation of sulfhydryls and hydroxyls. Lo et al. [28] also studied the adsorption of H_2S on the γ-Al_2O_3 surfaces, including the dehydrated and hydrated surfaces. They found that the chemisorption of H_2S on dehydrated surfaces is highly favored, while the phenomenon of physisorption is more likely to occur on the hydroxyl surfaces. Furthermore, H_2S adsorption on the dehydrated surface is more energetically favorable than the hydrated surface. Although the adsorption properties of H_2S on γ-Al_2O_3 surfaces have been characterized experimentally and theoretically, a detailed sulfurized mechanism has not been reported to date.

In this study, based on DFT together with periodic model, we systematically investigate the adsorption energies and geometries of H_2S and resultant species on the different γ-Al_2O_3 surfaces, including partially hydrated (110) surfaces, dehydrated (100) and (110) surfaces. The reaction processes and potential energy surfaces of H_2S decomposition on the different surfaces are also calculated, which may be advantageous to understand the reaction state of H_2S under different

RSC Advances Accepted Manuscript

operating environment and develop the new-style desulfurizers.

2. Computational methods and models

2.1. Calculation methods

All Kohn–Sham DFT calculations were performed using periodic model and a plane-wave basis set, as implemented in the Vienna ab initio simulation package (VASP).[29, 30] The interaction between valence electrons and the core was described by the full-potential projector augmented wave (PAW) method.[31, 32] The generalized gradient approximation (GGA) formulation of Perdew, Burke and Enzerhoff (PBE) [33] was employed to treat exchange-correlation energy. Brillouin zone integration was converged with a 3×3×1 k-point mesh generated by the Monkhorst-Pack algorithm.[34] The previous calculations had also shown that the 3×3×1 k-point mesh was sufficient to gain good converged results.[35, 36] Meanwhile, in order to guarantee the reliability of the 3×3×1 k-point mesh, the 3×3×1 k-point mesh was studied (see Table S1 in Supporting Information), it can be seen that the adsorption energies and activation energy is similar with each other. Therefore, we used the 3×3×1 k-point mesh. A cutoff energy of 400 eV was sufficient to obtain a satisfactory convergence of the total energy. In the structure optimization and energy calculation, the convergence tolerance was set to 10^{-5}eV for electronic self-consistent iteration and the residual forces of free atoms were limited smaller than 0.03 eV/Å. A Gaussian smearing function with a width of 0.1 eV was utilized to speed up convergence of the total energy. Spin polarization was used in all calculations. The transition states (TSs) and the minimum energy paths (MEPs) were located using the nudged elastic band (NEB) method.[37, 38] Eight equally spaced images were linearly interpolated between the reactant and final states. The quasi-Newton algorithm was used to relax the ion positions in all NEB calculations. All reported transition structures were verified to

RSC Advances Accepted Manuscript

exhibit only one imaginary frequency by the frequency calculations.

2.2. Surface models

The crystallographic bulk structure of γ-Al_2O_3 is complex and controversial because of the diversity of metastable phases during the preparation process. As far as we know, three typical γ-Al_2O_3 structures have been reported, including the traditional defective spinel structure,[39] the Paglia structure,[40] and the Digne structure.[41] In particular, the Digne structure is widely used in industrial catalysis applications.[42-44] Thus, the Digne structure of γ-Al_2O_3 is chosen for this study. The (110) and (100) surfaces are the main surfaces of γ-Al_2O_3, and contribute to approximately 90% of the overall surface area.[45] In the medium-high temperature desulfurization environment, [46, 47]the two surfaces are shown to form the different coverage of surface hydroxyls. According to the report of Digne et al. ,[45] the (100) surface is fully dehydrated above the Claus reaction conditions(~600 K), and the (110) surface contains 8.9 OH nm^{-2}, 5.9 OH nm^{-2} or 3.0 OH nm^{-2} in the temperature range from 600 K to 1150 K. Therefore, the present study will focus on dehydrated (100) and (110) as well as partially hydrated (110) surfaces including 3.0 OH nm^{-2}, 5.9 OH nm^{-2}, and 8.9 OH nm^{-2} surfaces. The (100) and (110) surfaces were modeled using a p(2 × 1) supercell and a p(1 × 1) supercell, respectively. In the case of the (100) surface, a four-layer slab was employed, where the two surface layers were relaxed and the bottom two layers were kept fixed in their bulk position. In the case of the (110) surface, the slab consisted of five atomic layers, where the bottom two layers were frozen to the bulk parameters and the remaining were allowed to relax. In all calculations, adsorbates were placed on one side of the slab, and a 15 Å thick vacuum spacer was inserted in the perpendicular direction to separate the surface slab.

The adsorption energy, E_{ad}, was defined as

RSC Advances Accepted Manuscript

$$E_{ad} = E_{(ads/slab)} - E_{(slab)} - E_{(ads)}$$

where $E_{(ads/slab)}$ represents the total energy of slab with the adsorbate, $E_{(slab)}$ represents the energy of the slab, and $E_{(ads)}$ represents the energy of the free adsorbate. Based on this definition, a negative E_{ad} value indicates exothermic adsorption, and the more negative value refers to the stronger exothermic interaction between adsorbate and slab.

The reaction energy (ΔE) and the activation energy (E_a) are defined as

$$\Delta E = E_{(FS)} - E_{(R)}$$

$$E_a = E_{(TS)} - E_{(R)}$$

Where $E_{(FS)}$, $E_{(R)}$, and $E_{(TS)}$ are, respectively, the total energy of the final state, of the reactant, and of the transition state in each elementary reaction.

3. Results and discussion

3.1 Bulk γ-Al_2O_3 and gas-phase H_2S and HS in vacuum.

In the present study, the bulk structure of γ-Al_2O_3 is monoclinic, and the unit cell contains 8 Al_2O_3 units. The cell volume after structure optimization is 369.13 $Å^3$ (46.14 $Å^3/Al_2O_3$ unit, namely, the cell volume per Al_2O_3 unit), which is about 0.54% smaller in comparison with the experimental value(46.39 $Å^3/Al_2O_3$ unit).[48] The corresponding lattice parameters after geometry optimization are a = 5.52 Å, b = 8.33 Å, c= 8.02 Å, and β= 90.62°. The largest deviation of these values is slightly less(1.08%) in comparison with the experimental value reported by Krokidis et al. .[49] Meanwhile, the relevant results of gas-phase H_2S and HS in vacuum, including bond lengths, bond angles, and vibrational frequencies, are summarized in Table 1. These calculated values are consistent with previous experimental and calculational data.[50-52]

3.2 Adsorption geometries and energies on the γ-Al_2O_3 surfaces.

RSC Advances Accepted Manuscript

Figure 1 shows the stable configurations of the dehydrated model γ-Al_2O_3 (100) and (110) surfaces, and the potential adsorption sites, which are used to investigate the interaction with possible adsorbates. For the purposes of discussion, the Al and O atoms in the outmost layer of the slab are labeled with I, II, III, IV and A, B, C, D, respectively. On the dehydrated γ-Al_2O_3 (100) surface, Al(I)–Al(III) exposed on the surface are pentacoordinated, while Al(IV) is tetracoordinated and in a position below the surface plane which is not available for adsorption.[53] All the O atoms are tricoordinated and labeled for the different marks because of different chemical environments. In the case of the dehydrated γ-Al_2O_3 (110) surface, the Al(I) and Al(II) atoms are tetracoordinated but have different chemical environments, and Al(III) is tricoodinated. The O(A) and O(B) atoms are tricoodinated, and the O(C) and O(D) atoms are dicoordinated. The geometries of partially hydrated (110) surfaces are shown in Figure 2, which include the 3.0, 5.9, and 8.9 OH nm^{-2} surfaces. In particular, the sites on the partially hydrated (110) surfaces equally use the marks of dehydrated surface.

3.2.1 Adsorption of H_2S, HS, S, and H on the dehydrated γ-Al_2O_3 (100) surface.

The optimized adsorption structures of H_2S, HS, S and H on the dehydrated γ-Al_2O_3 (100) surface are displayed in Figure 3, and the corresponding adsorption energies and geometric parameters for all adsorbates are summarized in Table 2. Similar to other metal oxides, H_2S can be adsorbed through the S atom on the metal cation, due to S lone-pair electrons.[54, 55] The H_2S molecule preferentially adsorbs on the Al(III) site, and the plane of H_2S molecule is nearly parallel to the surface. The bond distance of S–Al(III) is 2.657 Å, and the adsorption energy is –32.52 kJ/mol, which is in agreement with the result by Ionescu et al(–37 kJ/mol).[56] Meanwhile, the H–S bond lengths are stretched from 1.349 Å in the gas phase to 1.354 and 1.353 Å in the adsorbed

RSC Advances Accepted Manuscript

state, respectively. Likewise, HS is also favorably absorbed on the Al(III) site with an adsorption energy of –96.48 kJ/mol, and the S–Al(III) distance is 2.425 Å. These values reveal that the HS has the more strongly bonding capability with the surface compared to that of H_2S. In the case of S adsorption, the most stable configuration is located at the Al(III)–O(D) bridge site, which is similar to S adsorbed on the "Ce–O bridge" site on the CeO_2 surface.[57] The O–S and Al–S bond lengths are 1.788 and 2.388 Å, and the corresponding adsorption energy is –256.26 kJ/mol. Regarding H adsorption, the H atom readily adsorbs on the O site which has two stable adsorption structures, seeing H(a) and H(b) of Figure 3. In H(a) and H(b), the H atoms adsorb on O(C) and O(D) sites, respectively. The calculated adsorption energies are –143.49 and –143.55 kJ/mol on the O(C) and O(D) sites, and the bond lengths are 0.983 and 0.981 Å, respectively.

3.2.2. Adsorption of H_2S, HS, S, and H on the dehydrated γ-Al_2O_3 (110) surface.

As to the adsorption of H_2S, the optimized adsorption structure is displayed in Figure 4. In this configuration, the S atom of H_2S locates on the Al(III) site, yielding an adsorption energy of –114.38 kJ/mol. This adsorption energy is lower than that of the value obtained on the (100) surface by 81.86 kJ/mol, which reflects the stronger interaction between H_2S and (110) surface. The bond length of S–Al(III) is 2.417 Å, and two H–S bonds of adsorbed H_2S are elongated to 1.454 and 1.355 Å, respectively. It is obvious that the change of HS bond lengths can be attributed to the induction of coordinatively unsaturated Al cation for S and O anion for H. Similar to H_2S, the preferential adsorption site of HS is unsaturated Al(III) site, and the adsorption energy is –208.75 kJ/mol. For S adsorption, S atom is adsorbed on the Al(III)–O(C) or Al(I)–O(B) site to form two stable configurations [S(a) and S(b)], and the adsorption energies are –308.75 and –318.59 kJ/mol, respectively. The corresponding S–O and S–Al bonds are 1.765 and 2.263 Å,

RSC Advances Accepted Manuscript

1.741 and 2.224 Å, respectively. Regarding H adsorption, the optimized adsorption structure is that the H atom sits on the O(C) site with an adsorption energy of –340.80 kJ/mol and a bond distance of 1.091 Å. As seen from Table 2, the bonding strengths of these species on the (110) surface are stronger than those of on the (100) surface.

3.2.3. Adsorption of H_2S, HS, S, and H on the partially hydrated γ-Al_2O_3 (110) surfaces.

The most stable adsorption configurations for H_2S, HS, S and H on the partially hydrated surfaces are shown in Figure 5, and the corresponding adsorption energies and geometric parameters are summarized in Table 2. For H_2S, the H_2S still occupies the Al site with an S bond on the surface. The S–Al distances are 2.430, 2.586 and 2.540 Å, and the adsorption energies are –92.82, –39.85 and –67.57 kJ/mol on the 3.0, 5.9, and 8.9 OH nm^{-2} surfaces, respectively. It is found that the H–S bond lengths of H_2S on these surfaces are longer than that of the free H_2S, indicating H_2S is activated. The calculated values of adsorption energies show that the bonding strength of H_2S on the dehydrated surface is smaller than that of on the dehydrated surface (–114.38 kJ/mol). Clearly, surface water has influence on the chemical environment of intrinsic adsorption sites and changes the stable adsorption configurations of H_2S on these surfaces. It is to note that the adsorption energy on the 8.9 OH nm^{-2} surface is as much as 27.72 kJ/mol lower than that of on the 5.9 OH nm^{-2} surface(–67.57 vs –39.85 kJ/mol), which is consistent with the surface multimolecular adsorption of H_2S.[58]

In terms of HS adsorption on the 3.0 OH nm^{-2} surface, the HS steadily absorbs on two adjacent Al(I) atoms via the bridge bond mode[see Figure 5 HS], and the corresponding adsorption energy is –154.79 kJ/mol. Similar to the HS adsorption on the the 3.0 OH nm^{-2} surface, the S atom of HS is in direct contact with the both Al(I) sites on the 5.9 OH nm^{-2} surface.

RSC Advances Accepted Manuscript

However, as the bridge site occupied the HS favorably absorbs on the single Al(I) site and its H atom lies toward the O(A) site on the 8.9 OH nm^{-2} surface.

For S adsorption on the 3.0 OH nm^{-2} surface, the S atom binds to the surface Al(I) and O(B) atoms via the bridge bond mode forming the stable structure, as shown in Figure 5, and the absorption energies of which is –318.41 kJ/mol. Likewise, the S atom binds with the Al(I)–O(B) bridge site is still stable on the 5.9 OH nm^{-2} surface with adsorption energies of –307.44 kJ/mol, and the bond lengths of S–Al(I) and S–O(B) are 2.223 and 1.738 Å, respectively. Different from the 3.0 OH nm^{-2} and 5.9 OH nm^{-2} surfaces, the S atom preferentially occupies the O(A) site with a S bond on the 8.9 OH nm^{-2} surface with an absorption energy of –258.12 kJ/mol, which is 57.03 kJ/mol lower than that on Al(I)–O(B) bridge site. In contrast, surface hydroxyl adsorbed inhibits the S adsorption on the Al(I)–O(B) bridge site.

In the case of H adsorption, the optimal adsorption sites are O(C) on the 3.0 OH nm^{-2} surface, and O(A) on the 5.9 and 8.9 OH nm^{-2} surfaces, as illustrated in Figure 5, and the corresponding adsorption energies are –269.73, –268.15, and –273.33 kJ/mol, respectively. These absorption energy values are higher approximately 70 kJ/mol compared with the dehydrated surface. This indicates that the bonding strength of the H adsorption is weaker than that of the dehydrated surface.

3.3 Reaction mechanism of H_2S/γ-Al_2O_3 interactions.

The probable potential energy profiles of H_2S interacting with the γ-Al_2O_3 surfaces are constructed for the Figure 6, and the calculated values of reaction energy and activation energy for each elementary step are given. Figure 6(a) shows the first dehydrogenation process ($H_2S \rightarrow HS+H$), and the second dehydrogenation step ($HS \rightarrow H+S$) is displayed in Figure 6(b). The

RSC Advances Accepted Manuscript

relative structures on this potential energy profiles are depicted in Figure 7, 8 and 9, which include final states (FSs) and TSs on the different γ-Al_2O_3 surfaces. In addition, the coadsorption energies of FSs are also given in the Table 2. In particular, the reaction of H_2S on hydrated (110) surfaces will never involve desorption of H_2O prior to S–H activation due to the high adsorption energy of H_2O, similar to the CH_4 dissociation on the hydrated γ-Al_2O_3 surfaces.[44]

3.3.1 Dehydrated γ-Al_2O_3 (100) surface.

In the first dissociation step of H_2S, the most stable adsorption configuration of H_2S is selected as the initial state(IS), seeing H_2S in Figure 3. Along the dissociation process (H_2S→HS+H), the H–S bond is broken via $TS1_a$ leading to HS+H($FS1_a$) with a small activation energy of 13.22 kJ/mol. In contrast, a reaction barrier of 4.82 kJ/mol is needed to overcome on the CeO_2 (111) surface,[59] whereas the higher energy barrier of 52.40 kJ/mol surmounted on the Cu_2O (111) surface.[60] As presented in Figure 7, the breaking H–S bond in $TS1_a$ is 1.510 Å, which approximately elongates 0.156 Å compared to that in the IS. Nevertheless, the Al–S bond is shortened from 2.657 Å in IS to 2.462 Å in $TS1_a$. In $FS1_a$, the H atom absorbs on the O(C) site with a bond distance of 1.016 Å, and HS occupies the Al(III) site which is similar to the adsorption mode of single HS. The dehydrogenation process and coadsorption structure($FS1_a$) are similar to the H_2O dissociation on the γ-Al_2O_3 (100) surface.[61] It is found that the adsorption energy of coadsorption structure is much lower than the sum of the individual fragments on the surface. The origin of this effect has been attributed to charge transfer between the adsorbates through the support, which is consistent with the results of Christiansen et al. [61] and Huang et al. [62] . In this step, the energy released is close to 17.49 kJ/mol.

In terms of the second dissociation step, the HS can undergo the dehydrogenation process

RSC Advances Accepted Manuscript

(HS→H+S) forming H+S($FS2_b$) by overcoming an activation energy of 51.60 kJ/mol in $TS2_b$, as shown in Figure 6(b). This calculated value of activation energy is as much as 38.38 kJ/mol higher than that of the first dissociation step. This result indicates that this dissociation step is slightly difficult compared to the first dissociation step. Therefore, this step is the rate determining step in the dissociation reaction. By this reaction, the Al–S and H–S bond distances change from 2.425 and 1.354 Å in the HS to 2.322 and 1.511 Å in the $TS2_b$ and finally reaching to 2.272 and 1.987Å in the dissociation state ($FS2_b$), respectively. In $FS2_b$, the H and S atoms occupy on the O(C) and Al(III) sites, respectively, with a coadsorption energy of –652.14 kJ/mol.

3.3.2. Dehydrated γ-Al_2O_3 (110) surface.

In the IS, the H–S bond of H_2S can be completely activated elongation (1.454 Å vs 1.349 Å in the gas-phase), seeing H_2S in the Figure 4. Thus, the configurations of HS+H ($FS1_c$) can be formed via $TS1_c$ overcoming a 4.31 kJ/mol activation energy. The reaction energy of this step is –20.21 kJ/mol. In $FS1_c$, the HS still occupies on the Al(III) site and the H atom attaches the O(B) site with the bond distances of 1.028 Å. The breaking H–S and forming H–O bonds are 1.540 and 1.424 Å in the $TS1_c$, respectively. It is obvious that the first dissociation step is easy to occur due to the low activation energy.

The further dehydrogenation can take place via $TS2_d$ to form surface atomic S and another H atom. In $TS2_d$, the H–S bond is stretched to 1.626 Å from 1.354 Å in HS(see in Figure 4). The activation energy is 77.31 kJ/mol, which increases 73.00 kJ/mol compared with the parameter of $TS1_c$. After the $TS2_d$, the dissociative H atom attaches the O(C) site, and the S atom diffuse the Al(II)–Al(III) bridge site from the Al(III) site, forming the structure of $FS2_d$ which is similar to the dissociative adsorption geometry of HCN on the γ-Al_2O_3 (110) surface.[63] By comparing the stable

RSC Advances Accepted Manuscript

adsorption sites of the species between coadsorption structure(see Figure 8 $FS2_d$) and single optimal adsorption structure[see Figure 4 S(a)], it can be found that the most stable coadsorption site is not the superposition of every single optimal adsorption site. The detailed structural parameters are depicted in the Figure 8.

3.3.3. Partially hydrated γ-Al_2O_3 (110) surfaces.

To further understand the effect of hydrated surfaces for the H_2S removal, we also calculate the dissociation of H_2S on 3.0 OH nm^{-2}, 5.9 OH nm^{-2}, and 8.9 OH nm^{-2} surfaces. The corresponding structures of TSs and FSs along reaction paths are depicted in Figure 9.

For H_2S dissociation on the 3.0 OH nm^{-2} surface, based on the most stable adsorption structure of H_2S [see Figure 5 (3.0 OH nm^{-2} surface) H_2S] in which the H–S bond is elongated (1.380 Å vs 1.349 Å in the gas-phase) toward the surface O(C) site, the reaction starts from the approaching of the H to the O(C) site. By this reaction, the H–S bond distances change from 1.380 Å in the IS to 1.543 Å in the $TS1_e$ and finally reaching to 1.989Å in the $FS1_e$. In $FS1_e$, the produced O–H bond is 1.049 Å. The calculated activation energy is 6.73 kJ/mol which is smilar with that of the dehydrated surface (4.31 kJ/mol), meanwhile, the reaction energies have little difference in these two surfaces(–10.03 vs –20.21 kJ/mol). As depicted in Figure 6(a), the activation energies of the first dehydrogenation on the 5.9 and 8.9 OH nm^{-2} surfaces are 29.19 and 5.23 kJ/mol, and the corresponding reaction energies are –42.44 and –31.20kJ/mol, respectively. It is obvious that this step is easy to occur kinetically and thermodynamically on these three surfaces.

Immediately following, the second dissociation step is investigated, and the potential energy profile is depicted in Figure 6(b). The HS [see Figure 5 (3.0 OH nm^{-2} surface)] can break the H–S

RSC Advances Accepted Manuscript

bond to produce $FS2_f$ via transition states $TS2_f$ with activation energy of 62.81 kJ/mol. In $TS2_f$, the breaking H–S and forming H–O bonds are 1.485 and 1.506 Å, respectively. After $TS2_f$, this H–O bond length reduces further and reaches 0.993 Å in $FS2_f$. This process is 38.93 kJ/mol exothermic. In the case of HS dissociation on the 5.9 OH nm^{-2} surface, the H atom is abstracted from HS via $TS2_h$ to form H+S($FS2_h$) with an activation energy of 92.06 kJ/mol and an exothermicity of 13.22 kJ/mol. On the 8.9 OH nm^{-2} surface, the calculated activation energy ($TS2_j$) for H–S bond scission from HS [see Figure 5 (8.9 OH nm^{-2} surface)] to produce $FS2_j$ is 38.32 kJ/mol with a reaction energy of 8.35 kJ/mol. In $TS2_j$, the H–S bond distance is 1.773 Å, which is stretched 0.407 Å compared with the one of HS (1.366 Å). Detailed structural parameters are shown in the Figure 9.

From the results mentioned above, it can be seen that the bonding strengths of sulfur-containing species on the dehydrated (110) surface are stronger than those of on the dehydrated (100) surface. As the coverage of surface hydroxyl on the (110) surface, the bonding strengths of H_2S on these surfaces are ranked in the following order: H_2S (adsorbed on D110) > H_2S (adsorbed on 3.0 OH nm^{-2} surface) > H_2S (adsorbed on 8.9 OH nm^{-2} surface) > H_2S (adsorbed on 5.9 OH nm^{-2} surface) > H_2S (adsorbed on D100). The adsorption energies of HS on three hydrated surfaces are nearly equal, and the bonding strengths are in the order: HS (adsorbed on D110) > HS (adsorbed on 5.9 OH nm^{-2} surface) ≈ HS (adsorbed on 8.9 OH nm^{-2} surface) ≈ HS(adsorbed on 3.0 OH nm^{-2} surface) > HS(adsorbed on D100). Comparing the activation energies of the rate-determining step (HS→H+S), it is found that the value on the 5.9 OH nm^{-2} surface is highest than that of on other surfaces and is smallest on the 8.9 OH nm^{-2} surface. It is noted that adsorption energy and dissociative activation energy of H_2S are non-linear relationship

RSC Advances Accepted Manuscript

on these three partially hydrated (110) surfaces. On the 3.0 OH nm^{-2} surface, the energy level of Al(II) site is stronger than that of Al(I), therefore, Al(II) site benefits the adsorption and activation of H_2S.[45, 64] On the 8.9 OH nm^{-2} and 5.9 OH nm^{-2} surface, the adsorption energy difference of H_2S is due to the hydrogen bonds because of the same adsorption site [Al(I) site]. The H–S bond lengths of H_2S are 1.362 and 1.416 Å on the 8.9 OH nm^{-2} surface, and the H–S bond lengths of H_2S are 1.352 and 1.396 Å on the 5.9 OH nm^{-2} surface. The result shows that the influence of hydrogen bonds on the 8.9 OH nm^{-2} surface is larger than that of on the 5.9 OH nm^{-2} surface. Therefore, the adsorption stability of H_2S on the 8.9 OH nm^{-2} surface is larger than that of on the 5.9 OH nm^{-2} surface. The bond lengths of H_2S on the 8.9 OH nm^{-2} surface is longer than that of on the 5.9 OH nm^{-2} surface, indicating the H_2S dissociation on the 8.9 OH nm^{-2} surface is easier than that of on the 5.9 OH nm^{-2} surface. The result is similar is similar to the CH_4 dissociation on the hydrated γ-Al_2O_3 (110) surfaces.[44] It seems to be reasonable that the reaction occurs in 600 K, which is in accordance with the Claus process. The highest activation energy is also only 92.06 kJ/mol, which is consistent with the result by Bishara et al (76 kJ/mol).[65] Therefore, H_2S can easily dissociate into S species on the involved γ-Al_2O_3 surfaces.

4. Conclusions

In this paper, the interactions of H_2S with γ-Al_2O_3 surfaces, including partially hydrated (110) surfaces, dehydrated (100) and (110) surfaces, have been investigated using DFT. The possible adsorption structures and reaction pathways for H_2S dissociation were identified. The reported data show that H_2S and HS prefer to adsorb on the Al site, S and H atoms preferentially locate on the Al–O bridge and O sites, respectively. The bonding strengths of these species on the dehydrated (100) surface are weaker than on the dehydrated (110) surface, which is in good

RSC Advances Accepted Manuscript

agreement with previous experiment. Because of the surface active sites occupied, the bonding strengths of H_2S on hydrated (110) surfaces are smaller than the one on the corresponding dehydrated surface.

In this dehydrogenation reaction, the activation energy of second dissociation step becomes higher compared to that of the first step. Therefore, the second step could be the rate-determining step for H_2S dissociation on these surfaces. Comparing with the dehydrated (110) surface, the presence of surface OH groups has impact on activation energies and reaction energies in H_2S dissociation reaction. It is pointed out that the 8.9 OH nm^{-2} surface creates the lowest activation energy for dissociating H_2S, which makes a positive effect to the desulfurization and is in accordance with the Claus reaction occured in 600 K. Apparently reasonable hydroxyl coverage is beneficial to removal of H_2S. Of course, compared to all the activation energies on these involved surfaces, the highest activation energy is merely 92.06 kJ/mol on the 5.9 OH nm^{-2} surface. The results show that H_2S decomposition is facile on these involved γ-Al_2O_3 surfaces, both thermodynamically and kinetically. It is also proved that the γ-Al_2O_3 desulfurizer is highly efficient for the removal of H_2S.

Acknowledgments

The authors gratefully acknowledge the financial support of this study by the National Natural Science Foundation of China (21406154), Natural Science Foundation of Shanxi (2013021007-5), Special/Youth Foundation of Taiyuan University of Technology (2012L041 and 2013T092).

RSC Advances Accepted Manuscript

References

1. X. Li, Y. Wang, Y. Lei and Z. Gu, *Rsc Advances*, 2012, 2, 2302-2307.
2. S. Vallejos, T. Stoycheva, F. E. Annanouch, E. Llobet, P. Umek, E. Figueras, C. Canè, I. Gràcia and C. Blackman, *RSC Advances*, 2014, 4, 1489-1495.
3. Y. S. Hong, Z. Zhang, Z. Cai, X. Zhao and B. Liu, *Energy & Fuels*, 2014, 28, 6012-6018.
4. J. J. Chen, W. W. Li, H. Q. Yu and X. L. Li, *AIChE Journal*, 2013, 59, 3824-3833.
5. R. He, F.-F. Xia, J. Wang, C.-L. Pan and C.-R. Fang, *Journal of hazardous materials*, 2011, 186, 773-778.
6. K. Guo, J. Wen, Y. Zhao, Y. Wang, Z. Zhang, Z. Li and Z. Qian, *Environmental science & technology*, 2014, 48, 6844-6849.
7. J. Butt, *Activation, deactivation, and poisoning of catalysts*, Elsevier, 2012.
8. M. Husmann, C. Hochenauer, X. Meng, W. d. Jong and T. Kienberger, *Energy & Fuels*, 2014, 28, 2523-2534.
9. X. Ren, L. Chang, F. Li and K. Xie, *Fuel*, 2010, 89, 883-887.
10. F. Yazdanbakhsh, M. Bläsing, J. A. Sawada, S. Rezaei, M. Müller, S. Baumann and S. M. Kuznicki, *Industrial & Engineering Chemistry Research*, 2014, 53, 11734-11739.
11. L. Neveux, D. Chiche, J. Perez-Pellitero, L. Favergeon, A.-S. Gay and M. Pijolat, *Physical Chemistry Chemical Physics*, 2013, 15, 1532-1545.
12. G. Buelna and Y. Lin, *Separation and purification technology*, 2004, 39, 167-179.
13. C. Apesteguia, S. Trevizan, T. Garetto, J. P. de los Reyes and J. Parera, *Reaction Kinetics and Catalysis Letters*, 1982, 20, 1-6.
14. B. Guo, L. Chang and K. Xie, *Industrial & Engineering Chemistry Research*, 2014, 53, 8874-8880.
15. O. Saur, T. Chevreau, J. Lamotte, J. Travert and J.-C. Lavalley, *Journal of the Chemical Society, Faraday Transactions 1: Physical Chemistry in Condensed Phases*, 1981, 77, 427-437.
16. T. Reshetenko, S. Khairulin, Z. Ismagilov and V. Kuznetsov, *International journal of hydrogen energy*, 2002, 27, 387-394.
17. W. C. Content, New Jersey: John Wiley & Sons, Inc, 2007.
18. A. R. Ferreira, M. J. Martins, E. Konstantinova, R. B. Capaz, W. F. Souza, S. S. X. Chiaro and A. A. Leitao, *Journal of Solid State Chemistry*, 2011, 184, 1105-1111.
19. P. S. Prasad, J. W. Bae, S.-H. Kang, Y.-J. Lee and K.-W. Jun, *Fuel Processing Technology*, 2008, 89, 1281-1286.
20. I. Desyatov, E. Paukshtis and A. Mashkina, *Reaction Kinetics and Catalysis Letters*, 1990, 41, 85-88.
21. A. Datta and R. G. Cavell, *The Journal of Physical Chemistry*, 1985, 89, 450-454.
22. Y. Okamoto, M. Ohhara, A. Maezawa, T. Imanaka and S. Teranishi, *The Journal of Physical Chemistry*, 1986, 90, 2396-2407.
23. R. Glass and R. Ross, *The Journal of Physical Chemistry*, 1973, 77, 2576-2578.
24. T. Slager and C. Amberg, *Canadian Journal of Chemistry*, 1972, 50, 3416-3423.
25. A. Travert, O. Manoilova, A. Tsyganenko, F. Maugé and J. Lavalley, *The Journal of Physical Chemistry B*, 2002, 106, 1350-1362.
26. C. Finstrom and C. Adams, *Journal of Catalysis*, 1962, 1, 235-243.

RSC Advances Accepted Manuscript

27. C. Arrouvel, H. Toulhoat, M. Breysse and P. Raybaud, *Journal of Catalysis*, 2004, 226, 260-272.
28. J. M. Lo, T. Ziegler and P. D. Clark, *The Journal of Physical Chemistry C*, 2011, 115, 1899-1910.
29. G. Kresse and J. Furthmüller, *Physical Review B*, 1996, 54, 11169.
30. G. Kresse and J. Furthmüller, *Computational Materials Science*, 1996, 6, 15-50.
31. P. E. Blöchl, *Physical Review B*, 1994, 50, 17953.
32. G. Kresse and D. Joubert, *Physical Review B*, 1999, 59, 1758.
33. J. P. Perdew, K. Burke and M. Ernzerhof, *Physical review letters*, 1996, 77, 3865.
34. H. J. Monkhorst and J. D. Pack, *Physical Review B*, 1976, 13, 5188.
35. J. Joubert, A. Salameh, V. Krakoviack, F. Delbecq, P. Sautet, C. Copéret and J. M. Basset, *The Journal of Physical Chemistry B*, 2006, 110, 23944-23950.
36. P. Hirunsit, K. Faungnawakij, S. Namuangruk and C. Luadthong, *Applied Catalysis A: General*, 2013, 460, 99-105.
37. G. Henkelman, B. P. Uberuaga and H. Jónsson, *The Journal of chemical physics*, 2000, 113, 9901-9904.
38. G. Mills, H. Jónsson and G. K. Schenter, *Surface Science*, 1995, 324, 305-337.
39. H. Knözinger and P. Ratnasamy, *Catalysis Reviews Science and Engineering*, 1978, 17, 31-70.
40. G. Paglia, C. Buckley, A. Rohl, B. Hunter, R. Hart, J. Hanna and L. Byrne, *Physical Review B*, 2003, 68, 144110.
41. M. Digne, P. Sautet, P. Raybaud, P. Euzen and H. Toulhoat, *Journal of Catalysis*, 2002, 211, 1-5.
42. A. Salameh, J. Joubert, A. Baudouin, W. Lukens, F. Delbecq, P. Sautet, J. M. Basset and C. Coperet, *Angewandte Chemie International Edition*, 2007, 46, 3870-3873.
43. X. Tan, X. Ren, J. Li and X. Wang, *RSC Advances*, 2013, 3, 19551-19559.
44. R. Wischert, P. Laurent, C. Copéret, F. o. Delbecq and P. Sautet, *Journal of the American Chemical Society*, 2012, 134, 14430-14449.
45. M. Digne, P. Sautet, P. Raybaud, P. Euzen and H. Toulhoat, *Journal of Catalysis*, 2004, 226, 54-68.
46. Z. Wang and M. Flytzani-Stephanopoulos, *Energy & fuels*, 2005, 19, 2089-2097.
47. Y. I. Yoon, M. W. Kim, Y. S. Yoon and S. H. Kim, *Chemical engineering science*, 2003, 58, 2079-2087.
48. S. Wilson, *Journal of Solid State Chemistry*, 1979, 30, 247-255.
49. X. Krokidis, P. Raybaud, A.-E. Gobichon, B. Rebours, P. Euzen and H. Toulhoat, *The Journal of Physical Chemistry B*, 2001, 105, 5121-5130.
50. S.-F. Peng and J.-J. Ho, *The Journal of Physical Chemistry C*, 2010, 114, 19489-19495.
51. G. Herzberg, *New York: Van Nostrand, Reinhold, 1966*, 1966, 1.
52. K. Huber and G. Herzberg, Van Nostrand Reinhold, New York, 1979.
53. Z. Zuo, W. Huang, P. Han, Z. Gao and Z. Li, *Applied Catalysis A: General*, 2011, 408, 130-136.
54. J. A. Rodriguez and A. Maiti, *The Journal of Physical Chemistry B*, 2000, 104, 3630-3638.
55. X. Chu, Z. Lu, Y. Zhang and Z. Yang, *International Journal of Hydrogen Energy*, 2013, 38, 8974-8979.
56. A. Ionescu, A. Allouche, J.-P. Aycard, M. Rajzmann and F. Hutschka, *The Journal of Physical*

RSC Advances Accepted Manuscript

Chemistry B, 2002, 106, 9359-9366.

57. H.-T. Chen, Y. Choi, M. Liu and M. Lin, *The Journal of Physical Chemistry C*, 2007, 111, 11117-11122.
58. C. Ren, X. Wang, Y. Miao, L. Yi, X. Jin and Y. Tan, *Journal of Molecular Structure: THEOCHEM*, 2010, 949, 96-100.
59. D. Marrocchelli and B. Yildiz, *The Journal of Physical Chemistry C*, 2012, 116, 2411-2424.
60. R. Zhang, H. Liu, J. Li, L. Ling and B. Wang, *Applied Surface Science*, 2012, 258, 9932-9943.
61. M. A. Christiansen, G. Mpourmpakis and D. G. Vlachos, *Acs Catalysis*, 2013, 3, 1965-1975.
62. W.-F. Huang, H.-T. Chen and M. Lin, *The Journal of Physical Chemistry C*, 2009, 113, 20411-20420.
63. S. Kim, D. C. Sorescu and J. T. Yates, *The Journal of Physical Chemistry C*, 2007, 111, 5416-5425.
64. G. Feng, C.-F. Huo, C.-M. Deng, L. Huang, Y.-W. Li, J. Wang and H. Jiao, *Journal of Molecular Catalysis A: Chemical*, 2009, 304, 58-64.
65. A. Bishara, O. Salman, N. Khraishi and A. Marafi, *International journal of hydrogen energy*, 1987, 12, 679-685.

RSC Advances Accepted Manuscript

Figure caption

Figure 1. The stable configurations of the dehydrated model γ-Al_2O_3 (100) and (110) surfaces: (a) (100) surface; (b) (110) surface. The I, II, III and IV labels refer to the Al sites, and the A, B, C and D stand for the O sites. (gray, Al; red, O).

Figure 2. The stable configurations of the model γ-Al_2O_3 (110) surfaces for different hydroxyl coverage: hydrated with θ= 3.0 OH nm^{-2}; hydrated with θ= 5.9 OH nm^{-2}; hydrated with θ= 8.9 OH nm^{-2}. (gray, Al; red, O; white, H).

Figure 3. The optimized geometric structures of H_2S, HS, S and H adsorbed on the dehydrated γ-Al_2O_3 (100) surface, respectively. Distances are given in Å. (gray, Al; red, O; yellow, S; white, H).

Figure 4. The optimized geometric structures of H_2S, HS, S and H adsorbed on the dehydrated γ-Al_2O_3 (110) surface, respectively. Distances are given in Å. (gray, Al; red, O; yellow, S; white, H).

Figure 5. The optimized geometric structures of H_2S, HS, S and H adsorbed on the partially hydrated γ-Al_2O_3 (110) surfaces, respectively. Distances are given in Å. (gray, Al; red, O; yellow, S; white, H).

Figure 6. Calculated probable potential energy profiles for the dissociation of H_2S and HS on dehydrated and partially hydrated γ-Al_2O_3 surfaces. [D100 surface, the dehydrated γ-Al_2O_3 (100) surface; D110 surface, the dehydrated γ-Al_2O_3 (110) surface]

Figure 7. The calculated transition states (TSs) and corresponding final states (FSs) for the dissociation of H_2S and HS on the dehydrated γ-Al_2O_3 (100) surface.Distances are given in Å.

RSC Advances Accepted Manuscript

(gray, Al; red, O; yellow, S; white, H).

Figure 8. The calculated transition states (TSs) and corresponding final states (FSs) for the dissociation of H_2S and HS on the dehydrated γ-Al_2O_3 (110) surface. Distances are given in Å. (gray, Al; red, O; yellow, S; white, H).

Figure 9. The calculated transition states (TSs) and corresponding final states (FSs) for the dissociation of H_2S and HS on partially hydrated γ-Al_2O_3 (110) surfaces. Distances are given in Å. (gray, Al; red, O; yellow, S; white, H).

Table 1. Geometrical parameters and vibrational frequencies of gas-phase H_2S and HS.

Table 2. Calculated adsorption energies and geometric parameters for all adsorbates on the γ-Al_2O_3 surfaces.

RSC Advances Accepted Manuscript

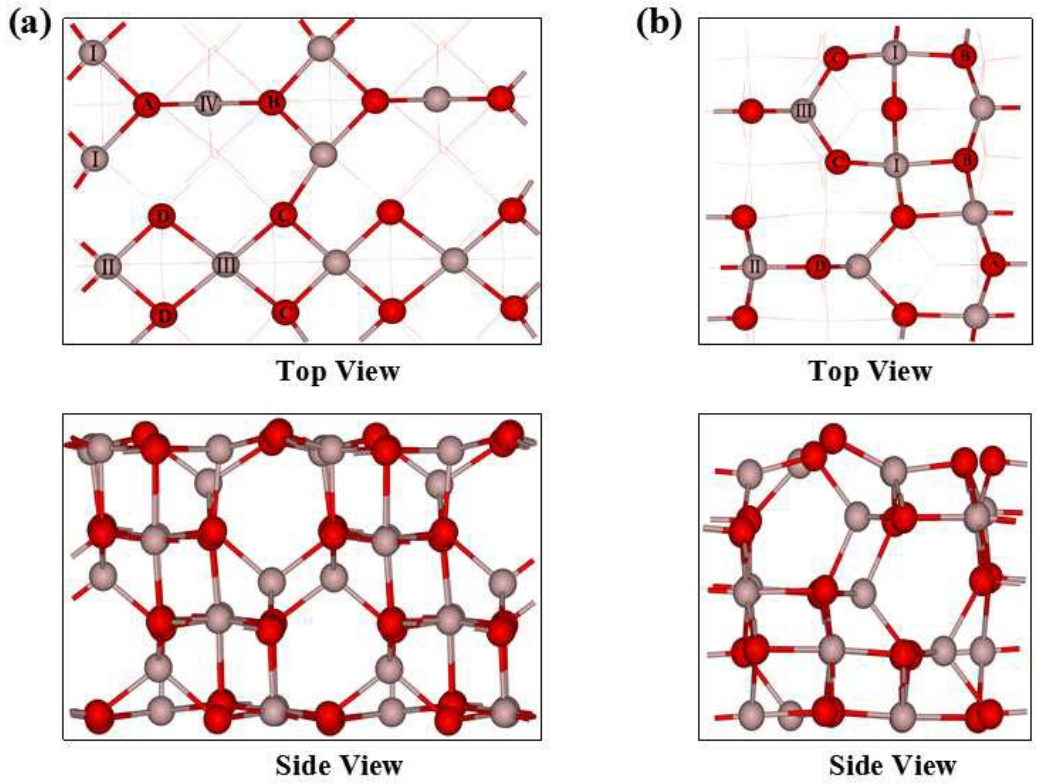

Figure 1. The stable configurations of the dehydrated model γ-Al_2O_3 (100) and (110) surfaces: (a) (100) surface; (b) (110) surface. The I, II, III and IV labels refer to the Al sites, and the A, B, C and D stand for the O sites. (gray, Al; red, O).

RSC Advances Accepted Manuscript

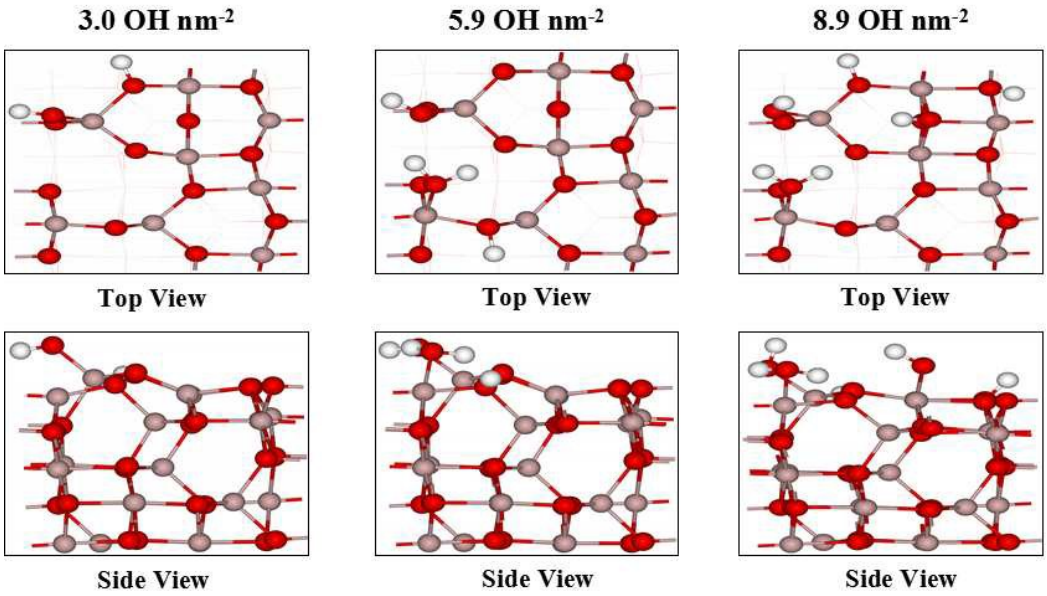

Figure 2. The stable configurations of the model γ-Al_2O_3 (110) surfaces for different hydroxyl coverage: hydrated with θ= 3.0 OH nm^{-2}; hydrated with θ= 5.9 OH nm^{-2}; hydrated with θ= 8.9 OH nm^{-2}. (gray, Al; red, O; white, H).

RSC Advances Accepted Manuscript

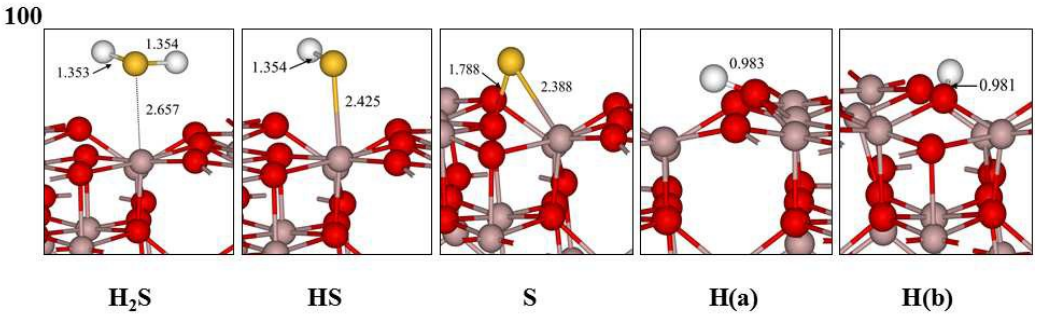

Figure 3. The optimized geometric structures of H_2S, HS, S and H adsorbed on the dehydrated γ-Al_2O_3 (100) surface, respectively. Distances are given in Å. (gray, Al; red, O; yellow, S; white, H).

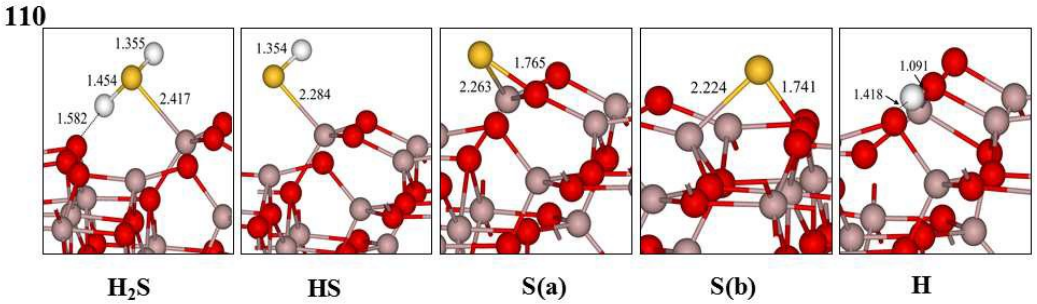

Figure 4. The optimized geometric structures of H_2S, HS, S and H adsorbed on the dehydrated γ-Al_2O_3 (110) surface, respectively. Distances are given in Å. (gray, Al; red, O; yellow, S; white, H).

RSC Advances Accepted Manuscript

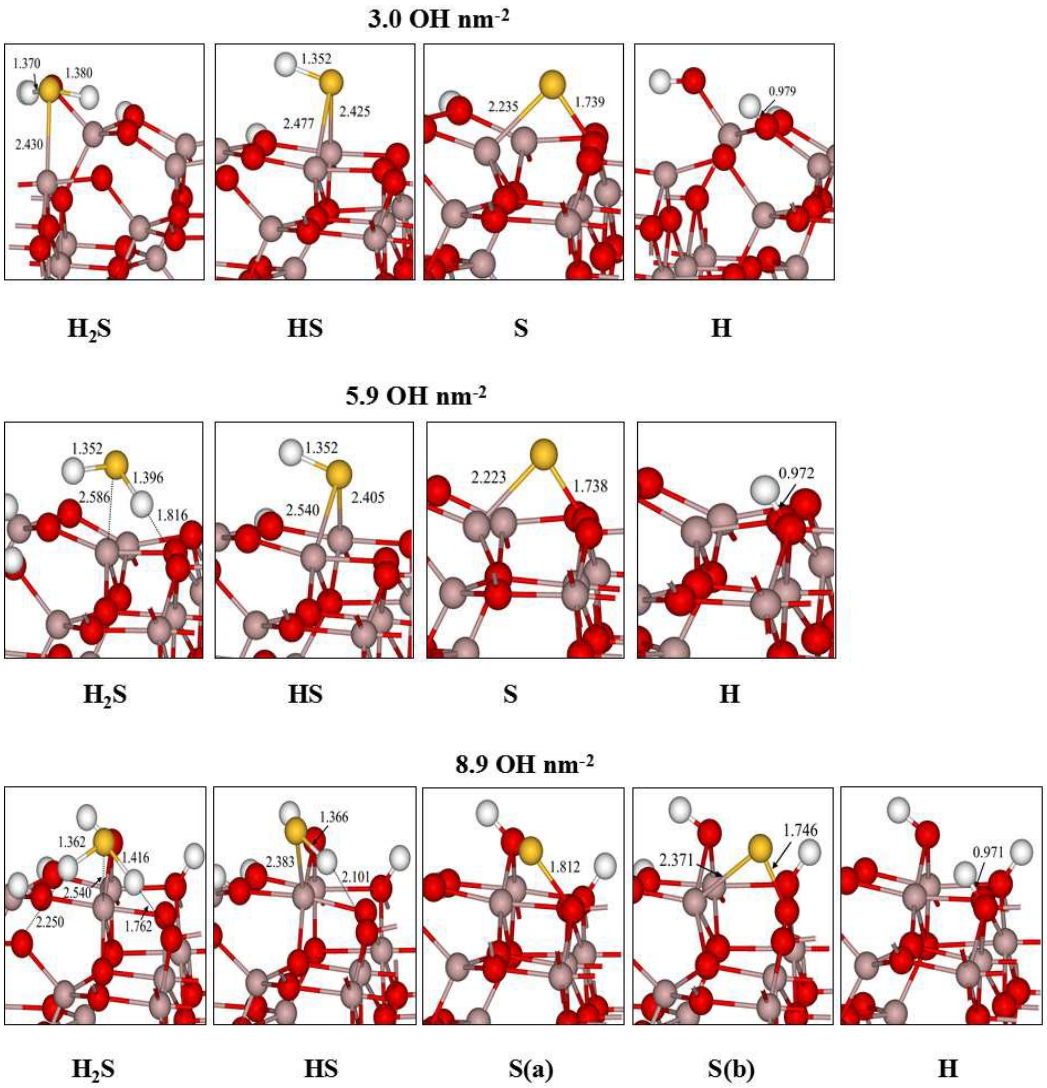

Figure 5. The optimized geometric structures of H_2S, HS, S and H adsorbed on the partially hydrated γ-Al_2O_3 (110) surfaces, respectively. Distances are given in Å. (gray, Al; red, O; yellow, S; white, H).

RSC Advances Accepted Manuscript

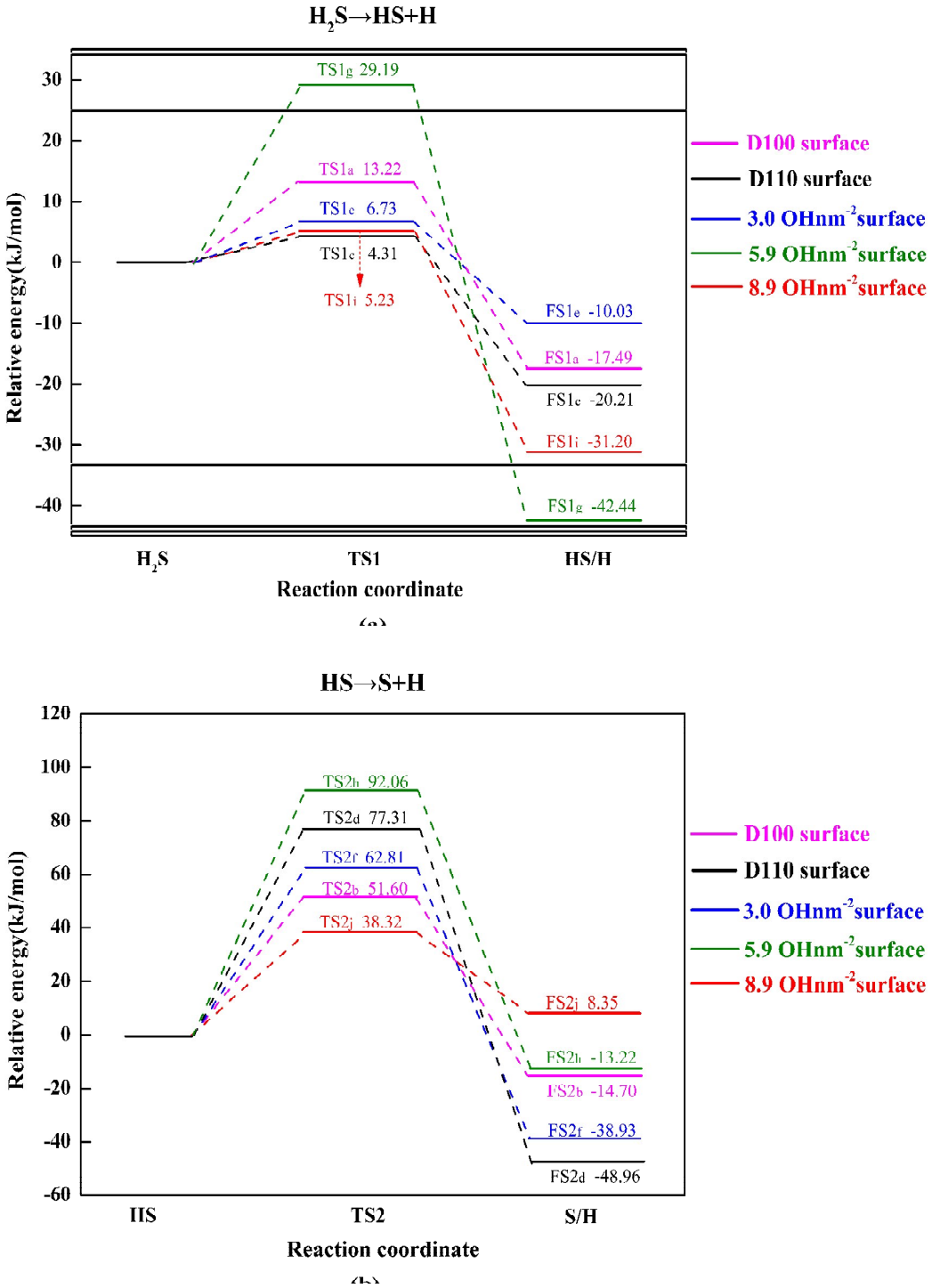

Figure 6. Calculated probable potential energy profiles for the dissociation of H_2S and HS on dehydrated and partially hydrated γ-Al_2O_3 surfaces. [D100 surface, the dehydrated γ-Al_2O_3 (100) surface; D110 surface, the dehydrated γ-Al_2O_3 (110) surface]

RSC Advances Accepted Manuscript

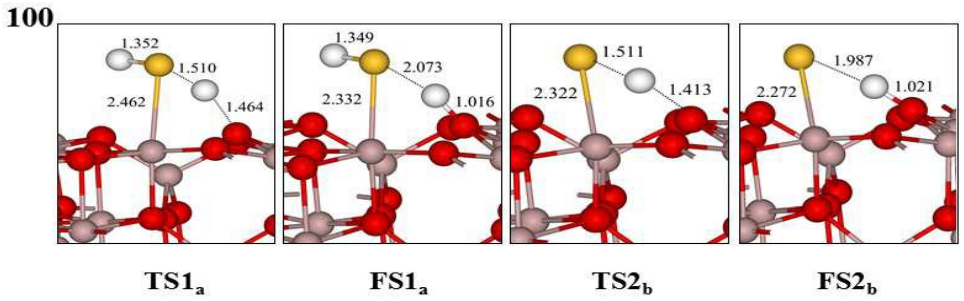

Figure 7. The calculated transition states (TSs) and corresponding final states (FSs) for the dissociation of H_2S and HS on the dehydrated γ-Al_2O_3 (100) surface. Distances are given in Å. (gray, Al; red, O; yellow, S; white, H).

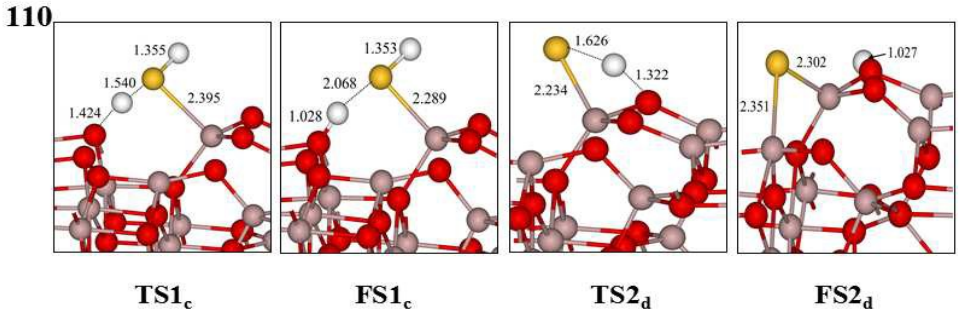

Figure 8. The calculated transition states (TSs) and corresponding final states (FSs) for the dissociation of H_2S and HS on the dehydrated γ-Al_2O_3 (110) surface. Distances are given in Å. (gray, Al; red, O; yellow, S; white, H).

RSC Advances Accepted Manuscript

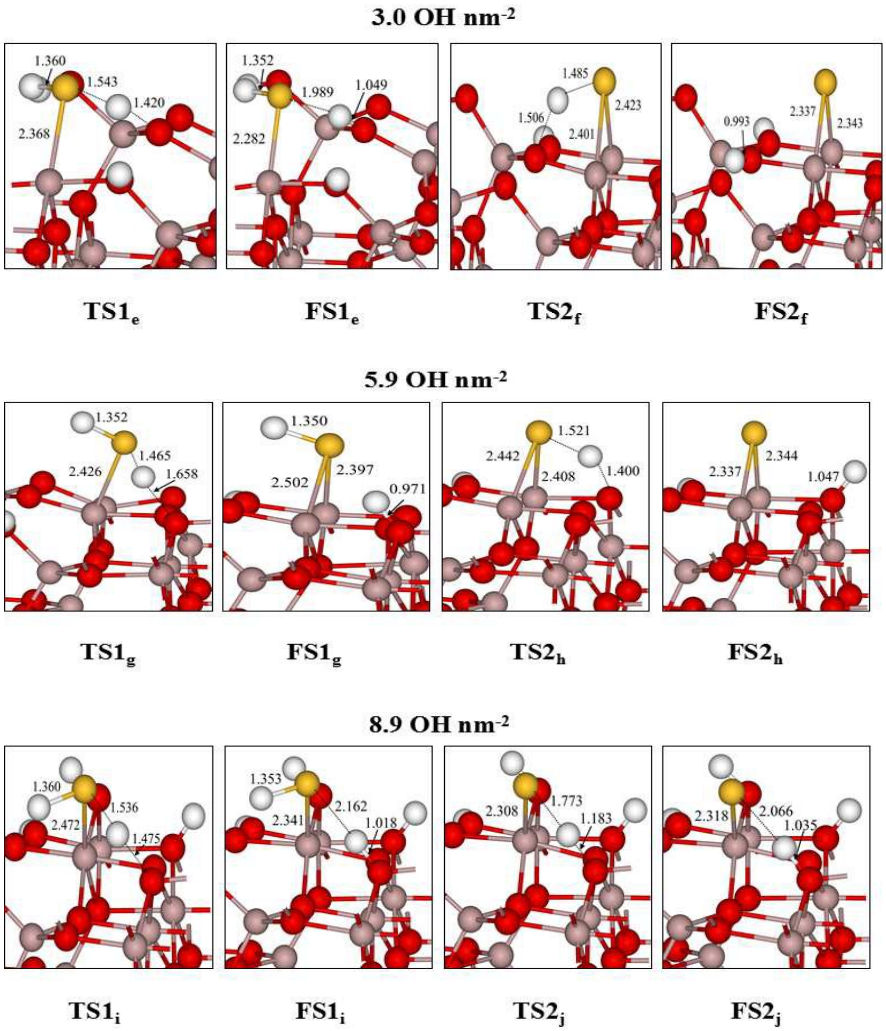

Figure 9. The calculated transition states (TSs) and corresponding final states (FSs) for the dissociation of H_2S and HS on partially hydrated γ-Al_2O_3 (110) surfaces. Distances are given in Å. (gray, Al; red, O; yellow, S; white, H).

RSC Advances Accepted Manuscript

Table 1. Geometrical parameters and vibrational frequencies of gas-phase H_2S and HS

	H_2S		HS	
	cal[a]	expt[b]	cal[a]	expt[c]
r(S–H) (Å)	1.349[1.337]	1.328	1.354[1.331]	1.346
θ(deg)	91.6[91.9]	91.6		
V_{asym} (cm^{-1})	2663[2673]	2628	2623[2634]	2660
V_{sym} (cm^{-1})	2643[2654]	2615		
γ_{bend} (cm^{-1})	1171[1172]	1183		

[a] Values in brackets are predicted from Ref.[50]

[b] From Ref.[51]

[c] From Ref.[52]

RSC Advances Accepted Manuscript

Table 2. Calculated adsorption energies and geometric parameters for all adsorbates on the γ-Al_2O_3 surfaces.

species	param[a]	D100[b]	D110[c]	3.0 OH nm^{-2} [e]	5.9 OH nm^{-2}	8.9 OH nm^{-2}
H_2S	site	**Al** III	**Al** III	**Al** II	**Al** I	**Al** I
	dH–S (Å)	1.354/1.353	1.454/1.355	1.380/1.370	1.396/1.352	1.416/1.362
	dS–Al(Å)	2.657	2.417	2.430	2.586	2.540
	∠HSH(deg)	91.0	95.0	90.6	94.7	94.1
	E_{ad}(kJ/mol)	–32.52	–114.38	–92.82	–39.85	–67.57
HS	site	**Al** III	**Al** III	**Al** I-I	**Al** I-I	**Al** I
	dH–S(Å)	1.354	1.354	1.352	1.352	1.366
	dS–Al(Å)	2.425	2.284	2.425/2.477	2.405/2.540	2.383
	E_{ad}(kJ/mol)	–96.48	–208.75	–154.79	–158.64	–155.06
S	site	**Al** III-**O**D	**Al** III-**O**C/**Al** I-**O**B	**Al** I-**O**B	**Al** I-**O**B	**O**A
	dS–O(Å)	1.788	1.765/1.741	1.739	1.738	1.812
	dS–Al(Å)	2.388	2.263/2.224	2.235	2.223	--
	E_{ad}(kJ/mol)	–256.26	–308.75/–318.59	–318.41	–307.44	–258.12
H	site	**O**C/**O**D	**O**C	**O**C	**O**A	**O**A
	dS–H(Å)	0.983/0.981	1.091	0.979	0.972	0.971
	E_{ad}(kJ/mol)	–143.49/–143.55	–340.80	–269.73	–268.15	–273.33
HS+H	E_{ad}(kJ/mol)	–587.55($FS1_a$)[d]	–672.14($FS1_c$)	–640.40($FS1_e$)	–619.84($FS1_g$)	–636.32($FS1_i$)
S+H	E_{ad}(kJ/mol)	–652.14($FS2_b$)	–798.68($FS2_d$)	–734.67($FS2_f$)	–712.82($FS2_h$)	–687.67($FS2_j$)

[a] param: parameters. [b] D100, the dehydrated γ-Al_2O_3 (100) surface; [c] D110, the dehydrated γ-Al_2O_3 (110) surface. [d] FS denotes the final state. [e] 3.0 OH nm^{-2}, 5.9 OH nm^{-2} and 8.9 OH nm^{-2} represent the different levels of hydroxyl coverage for γ-Al_2O_3 (110) surface.

RSC Advances Accepted Manuscript